SURVEY OF APPLICATIONS OF RADAR REFRACTIVITY RETRIEVALS

D. Bodine[1,2,*], P. L. Heinselman[3], R. D. Palmer[1,2], B. L. Cheong[2], and D.Michaud[1,2]

[1]School of Meteorology, The University of Oklahoma, Norman, OK, U.S.A.
[2]Atmospheric Radar Research Center, The University of Oklahoma, Norman, OK, U.S.A
[3]NOAA/OAR National Severe Storms Laboratory, Norman, OK, U.S.A

1. INTRODUCTION

The absence of small-scale moisture measurements near the surface is a major limitation in forecasting convective precipitation (Emanuel et al., 1995; Dabberdt and Schlatter, 1996; National Research Council, 1998). Recent breakthroughs in retrieving near-surface refractivity from weather radar are providing new opportunities for high-resolution, near-surface moisture measurements (Fabry et al., 1997; Fabry, 2004; Cheong et al., 2008). Refractivity retrievals obtained from the WSR-88D network can provide moisture measurements with very high spatial (as small as 2 km) and temporal resolution (4.2–10 minutes depending on volume coverage pattern). These measurements provide superior spatial resolution to the Automated Surface Observing System (ASOS), which has an average spacing of 90 km (Koch and Saleeby, 2001).

Several observational and modeling studies have shown that moisture variability plays an important role in convection initiation. Deep lifting of boundary layer moisture is needed for convection initiation, often occurring along strong moisture gradients such as the dryline (Ziegler et al., 1997; Ziegler and Rasmussen, 1998; Parsons et al., 2000). The Convection and Precipitation/Electrification (CaPE) project (Weckwerth et al., 1996; Weckwerth, 2000) focused on the impact of moisture variability on convection initiation in a quiescent environment. During the CaPE project, Weckwerth et al. (1996) found that differences in moisture between updraft and downdraft branches of horizontal convective rolls (HCRs) ranged from 1.5 to 2.5 g kg^{-1}. The CaPE project demonstrated that HCR updraft branches could sufficiently lower the level of free convection (LFC) and reduce the convective inhibition (CIN) to enable convection initiation through boundary layer forcing (Weckwerth, 2000). Using a combination of radar refractivity data and in-situ moisture measurements from aircraft obtained during the International H_20 Project (IHOP; Weckwerth et al., 2004), Fabry (2006) found that moisture variability had a greater effect on CIN compared to temperature variability at scales less than 20 km. Numerical simulations have also shown that convection initiation is sensitive to small changes in surface moisture (Lee et al., 1991; Crook, 1996). Simulations by Crook (1996) showed that changes in moisture as small as 1 g kg^{-1} determined if convection initiation would occur.

* *Corresponding author address:* David Bodine, University of Oklahoma, School of Meteorology, 120 David L. Boren Blvd., Rm 4630, Norman, OK 73072-7307; e-mail: bodine@ou.edu

Several papers have suggested potential applications for using radar refractivity retrievals to enhance short-term convection initiation forecasts (Fabry, 2004; Weckwerth et al., 2005; Fabry, 2006; Wakimoto and Murphey, 2008; Bodine et al., 2008). In initial tests of the refractivity retrieval algorithm near Montreal, Quebec, Fabry (2004) showed that the algorithm could provide accurate, near-surface refractivity measurements. Results from IHOP and the Oklahoma Refractivity Experiment (Heinselman et al., 2009) revealed the capability to use refractivity data to observe moisture changes associated with cold fronts, outflow boundaries, drylines, boundary layer structures, misocyclones, supercells, and tornadogenesis (Weckwerth et al., 2005; Fabry, 2006; Demoz et al., 2006; Buban et al., 2007; Roberts et al., 2008; Wakimoto and Murphey, 2008; Bodine et al., 2008, 2009a,b; Heinselman et al., 2009). Weckwerth et al. (2005) also showed that radar refractivity data could identify strengthening moisture gradients associated with a dryline before a fine line developed in reflectivity, and Roberts et al. (2008) presented a similar case where increasing moisture gradients along a convergent boundary preceded convection initiation. Though these studies have presented promising applications of radar refractivity retrievals, an operational evaluation of refractivity at the Norman, Oklahoma Weather Forecast Office (WFO) found that the participating forecasters did not obtain significant benefits from refractivity data, and gave low importance to implementing refractivity into the Advanced Weather Interactive Processing System, or AWIPS (Heinselman et al., 2009). One forecaster suggested that additional research is needed to identify new applications of refractivity data that provide new information to forecasters that cannot be obtained from the current observation network; in their case the Oklahoma Mesonet.

The objective of this study is to demonstrate the capability to use radar refractivity data to observe small-scale moisture variability important to convection initiation, and investigate its impact on convection initiation in a synoptically active environment. Most observational studies have focused on the impact of moisture variability on convection initiation in quiescent conditions (e.g., Weckwerth, 2000), or examined convection initiation cases with strong moisture gradients associated with boundaries (e.g., drylines, outflow boundaries). The convection initiation cases presented with radar refractivity retrievals have focused on cases involving boundaries characterized by increasing moisture gradients (Weckwerth et al., 2005; Roberts et al., 2008).

This study investigates applications of radar refractivity data by examining the surface moisture variability in the absence of strong moisture gradients and evaluating its impact on convection initiation. The study also addresses the need to demonstrate sub-observational-scale utility of radar refractivity data by presenting a case where radar refractivity data exhibited potential utility for short-term convection initiation forecasting.

Section 2 briefly describes the radar refractivity algorithm developed at the Atmospheric Radar Research Center (ARRC) at the University of Oklahoma, and presents a preliminary error analysis. The refractivity data and other data used in the case study are discussed in Section 3. The convection initiation case study is presented in Section 4. The synoptic and preconvective, mesoscale environments are described, and observations of the moisture variability from radar refractivity retrievals are presented. Then, the impact of moisture variability on convection initiation is investigated through sounding analyses. Section 5 presents a summary and discussion of the results.

2. RADAR REFRACTIVITY RETRIEVAL ALGORITHM

The ARRC has developed an independent algorithm for refractivity retrieval based on the work by Fabry et al. (1997). The University of Oklahoma algorithm has been adapted easily for different weather radars, including the Weather Surveillance Radar-1988 Dopplers (WSR-88Ds), the Collaborative Adaptive Sensing of the Atmosphere (CASA; McLaughlin et al., 2009) X-Band Radars, and the National Weather Radar Testbed (NWRT) Phased Array Radar (PAR; Zrnić et al., 2007), for example. Cheong et al. (2008) provide a detailed description of the University of Oklahoma refractivity algorithm, although it is briefly described here for completeness.

The refractive index, n, is often rewritten in terms of refractivity, N, to improve the ease of interpretation (Bean and Dutton, 1968);

$$N = (n-1) \times 10^6. \quad (1)$$

Bean and Dutton (1968) showed that refractivity could be related to temperature, pressure and water vapor pressure using the following equation,

$$N = 77.6\frac{p}{T} + 3.73 \times 10^5 \frac{e}{T^2}, \quad (2)$$

where *p* is pressure in millibars, *T* is the temperature in Kelvin, and *e* is the water vapor pressure in millibars. At warmer temperatures, refractivity provides a good approximation for surface moisture, as temperature and pressure changes affect refractivity less than moisture changes.

Radar refractivity retrievals are obtained using phase measurements between the radar and ground clutter targets. Reference phase measurements are made when the moisture field is nearly homogeneous and constant with time. At the same time, an objectively analyzed refractivity field is derived from Oklahoma Mesonet (Mesonet, hereafter) data (Brock et al., 1995; McPherson et al., 2007) to create a reference refractivity field. Real-time phase measurements are collected to produce a phase difference field using the reference and real-time phase measurements. Poor clutter targets are then censored based on clutter quality indices. The resulting phase difference field is relatively noisy and sparse, so the phase difference field is smoothed using a 2.5-km Gaussian window. Next, the radial derivative of the phase difference field is computed to obtain the refractivity change field. The resulting refractivity change field is subsequently smoothed to reduce the noise introduced by the derivative operation. Absolute refractivity (hereafter, refractivity) can be computed by adding the refractivity change and the reference refractivity fields. Scan-to-scan refractivity change (hereafter, scan-to-scan refractivity) is computed by substituting the phase measurements from the previous scan for the reference phase measurements, and applying the same procedure to the phase difference data.

A preliminary error analysis was conducted to evaluate the accuracy of radar refractivity retrievals derived from the OU algorithm. The Norman, Oklahoma (NRMN) Mesonet station was located within good refractivity coverage, so the NRMN station was selected for comparison (Fig. 1). Time-series of radar and NRMN refractivity were computed for the period from 22 April to 8 May 2007 (Fig. 2). The time-series plot shows good agreement between the radar and NRMN refractivity measurements, even during rapidly changing conditions (e.g., advancing and retreating drylines on 22–23 April 2007). The correlation coefficient between the Mesonet and radar refractivity measurements was 0.976, showing excellent correlation between the two measurements.

The refractivity bias, ϵ^i, was computed from refractivity and NRMN Mesonet refractivity data using the following equation,

$$\epsilon^i = N^i_{refrac} - N^i_{NRMN}, \quad (3)$$

where N^i_{refrac} and N^i_{NRMN} are the refractivity and NRMN Mesonet refractivity measurements at time i. The mean bias was -4.2 N-units for the period from 22 April to 8 May 2007. Even after removing the mean bias, the root-mean squared error was 3.2 N-units, primarily the result of the time-varying bias. The variability of the bias appears to be related to changes in the near-surface, vertical refractivity gradient. For this study, refractivity gradients and scan-to-scan refractivity are primarily used in the analysis, and these quantitates are affected significantly less by the time-varying bias. The ARRC is currently studying this bias problem and developing mitigation schemes.

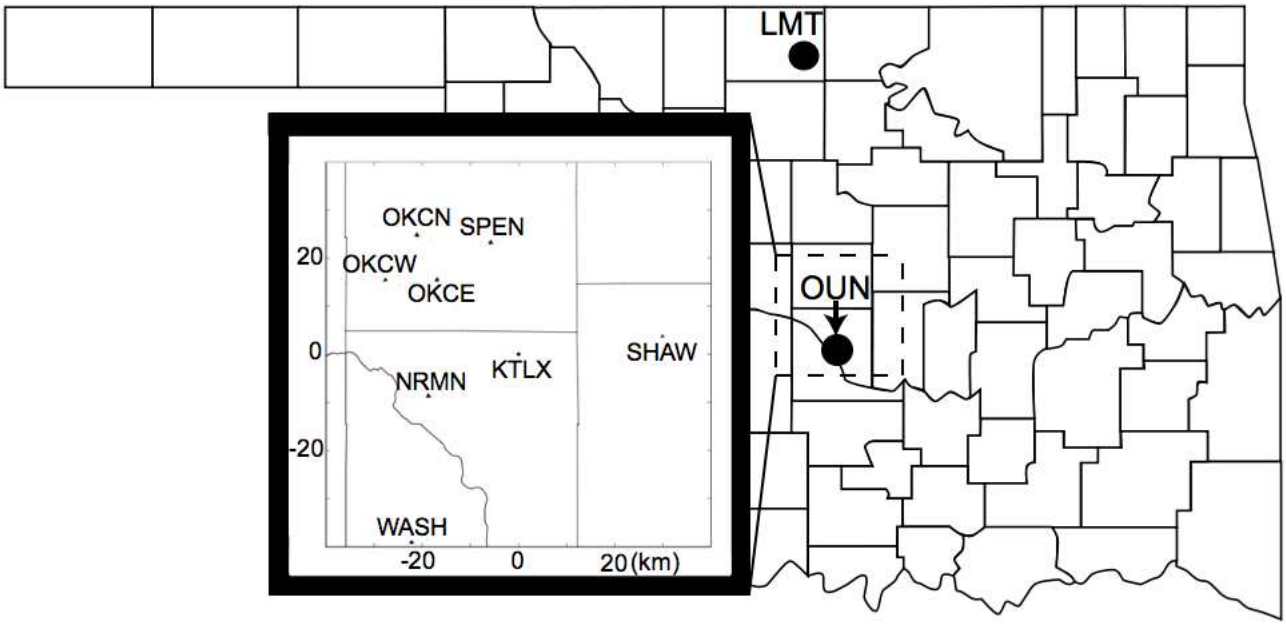

Figure 1: Plot showing the location of the sounding sites (OUN and LMT), KTLX, and Mesonet stations. The dashed box shows the approximate region of the KTLX refractivity domain, and large inset box shows the Mesonet stations within the domain.

3. DATA

Four radar products from the Twin Lakes, Oklahoma (KTLX) WSR-88D (Fig. 1) were analyzed throughout the study – reflectivity, radial velocity, velocity azimuth display (VAD), and refractivity data. For this case study, KTLX Level-II reflectivity, radial velocity, and Level-III VAD data were obtained for 1723–1816 UTC 30 April 2007. Storm motion and divergence were calculated from these products as needed. Storm motion was computed using the Warning Decision Support System – Integrated Information (WDSSII; Lakshmanan et al., 2007) display by tracking a well-defined structure within the storm between consecutive scans. Divergence, δ, was computed from the radial velocity, v_r, of two range gates, n and $n+k$, within the same azimuth angle, using

$$\delta = \frac{v_r^{n+k} - v_r^n}{\Delta r}. \quad (4)$$

The distance between range gates $n+k$ and n is given by Δr, which was 1 km for this study.

Volume Coverage Pattern (VCP) 32 was operating between 1723–1811 UTC, and VCP 11 was operating between 1811–1816 UTC. The refractivity data used in this study were collected during the KTLX Spring 2007 Refractivity Experiment (Heinselman et al., 2009). Refractivity data were collected from 8 April 2007 to 10 July 2007 from KTLX.

Throughout the experiment, refractivity data were compared with the Mesonet stations within the refractivity domain (Fig. 1). The Mesonet provides 5-min surface observations with approximately 35-km station spacing (Brock et al., 1995; McPherson et al., 2007). Using Mesonet relative humidity, pressure, and temperature measurements, Mesonet refractivity can be computed for comparison with radar refractivity.

Radiosonde data and Rapid Update Cycle (RUC; Benjamin et al., 2004) analyses were used to analyze the preconvective synoptic and mesoscale environments. Radiosonde data from Norman, Oklahoma (OUN; Fig. 1) were used to analyze the thermodynamic profile, and modified using the Skew-T/Hodograph Analysis Research Program (NSHARP; Hart and Korotky, 1991) to study the effects of moisture changes on the thermodynamic profile. Sounding data from the Lamont, Oklahoma (LMT; Fig. 1) sounding were also used for comparison. RUC analyses were used to identify synoptically favorable regions for convection initiation.

4. 30 APRIL 2007 CASE

An isolated storm developed near Oklahoma City, Oklahoma on 30 April 2007 shortly after 1800 UTC. The storm eventually produced 66-dBZ echoes at 1819 UTC, although no severe weather reports were received. This section presents an overview of the synoptic and mesoscale environment, a discussion of the ingredients in convection

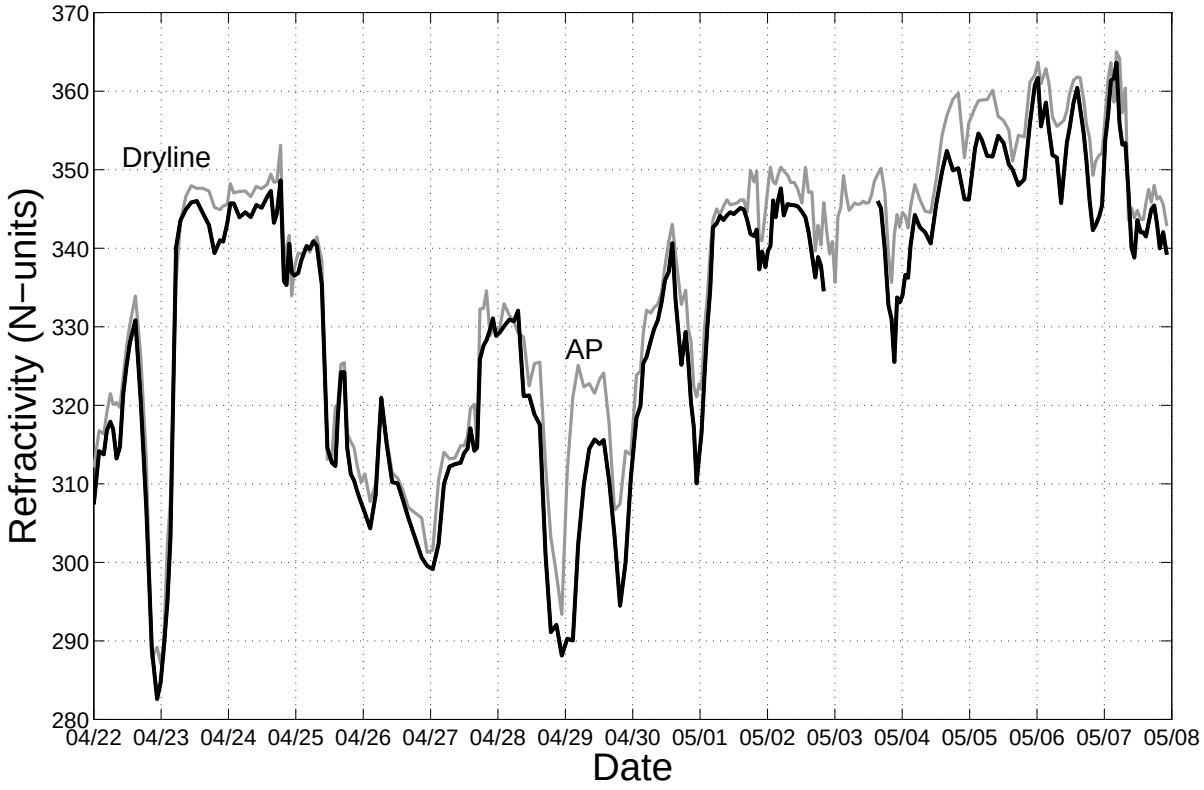

Figure 2: Time-series plot of radar refractivity (black line) and the Norman, Mesonet-derived refractivity (light gray line) between 22 April and 8 May 2007. The time-series plot shows excellent correlation between the Mesonet and radar refractivity measurements, even during rapidly evolving conditions such as an advancing and retreating dryline on 22–23 April 2007. A large bias often occurs in the early morning hours, possibly caused by anomalous propagation (AP). Radar refractivity data flow was interrupted between 2054 UTC 2 May and 1408 UTC 3 May 2007.

initiation, and an investigation of the impact of moisture variability on convection initiation.

4.1. Synoptic and Mesoscale Environment

The 1800 UTC 30 April 2007 RUC analysis showed that the convection initiation site (central Oklahoma) was situated between the 500-hPa short-wave trough axis located over western Texas and the 500-hPa short-wave ridge axis over southern Missouri and Arkansas (Fig. 3a). A 500-hPa cutoff low was centered over eastern New Mexico and the Texas Panhandle, and was collocated with a maximum in 500-hPa absolute vorticity (Fig. 3a). The region downstream from the cutoff low was favorable for upward motion at lower and midlevels owing to increasing positive vorticity advection between 850 and 500 hPa (not shown). The 1800 UTC RUC 700-hPa analysis revealed weak upward motion between -0.05 and -0.1 Pa s^{-1} over central Oklahoma (Fig. 3b), further suggesting that the region was favorable for synoptic-scale ascent.

The surface analysis from 1825 UTC showed a mesoscale boundary (MB), characterized by a weak temperature gradient (Fig. 3c). The source of the MB appeared to be a weak cold pool from on-going precipitation in southwest Oklahoma. The surface analysis showed the MB extending southward from central Oklahoma, with southwesterly winds west of the MB and southerly winds east of the MB (Fig. 3c). Small dewpoint temperature differences across the MB of about 2–3°C were also observed. At 1825 UTC, a line of convection was developing along the MB in southern Oklahoma, and an isolated storm was also developing along the MB near Oklahoma City (Fig. 3c).

Significant moisture variability was observed in refractivity (Fig. 4a) and scan-to-scan refractivity (Fig. 4b) in the area where the isolated storm developed. The moisture pool was most clearly depicted by scan-to-scan refractivity, which showed a region of positive scan-to-scan refractivity moving north-northeast at approximately 5 m s^{-1} (Fig. 4b). At 1755 UTC, the refractivity difference across the moisture pool was 10 N-units, and the corresponding difference in dewpoint temperature from the Mesonet was 2°C between the NRMN and Oklahoma City East (OKCE) Mesonet stations (Fig. 4a). Assuming constant temperature and pressure, a 2°C change in dewpoint temperature was equal to a 10 N-unit change in refractivity, showing good agreement between the Mesonet and radar refractivity observations. The radial velocity field relative to the moisture pool is discussed later (Fig. 4c). The left edge of the moisture pool passed over the NRMN and OKCE Mesonet stations and produced a small change in dewpoint temperature. As the moisture pool moved toward the northern fringe of the refractivity domain at 1811 UTC, the moisture pool was moving toward the Spencer, Oklahoma (SPEN) Mesonet station. Between 1820–1845 UTC, the dewpoint temperature rose from 14.8 to 16.2°C as the moisture pool passed over the SPEN Mesonet station (Fig. 5a), and the radar refractivity increased 5 N-units (Fig. 5b).

Although the lower and midlevel dynamics were favorable for synoptic-scale ascent, a mesoscale mechanism for low-level lift was necessary for convection initiation (e.g., Doswell, 1987). The MB provided a potential mechanism for low-level lift, and the MB was observed in the KTLX reflectivity and radial velocity fields. The moisture pool (Fig. 6a and b) was located west of a north-south-oriented fine line evident in the 0.5°-tilt reflectivity field at 1805 and 1815 UTC (Fig. 6c). Once the fine line developed, it showed temporal continuity between scans, and enhanced reflectivity at lower tilts. A more in-depth examination of the fine line associated with the MB follows in the next section.

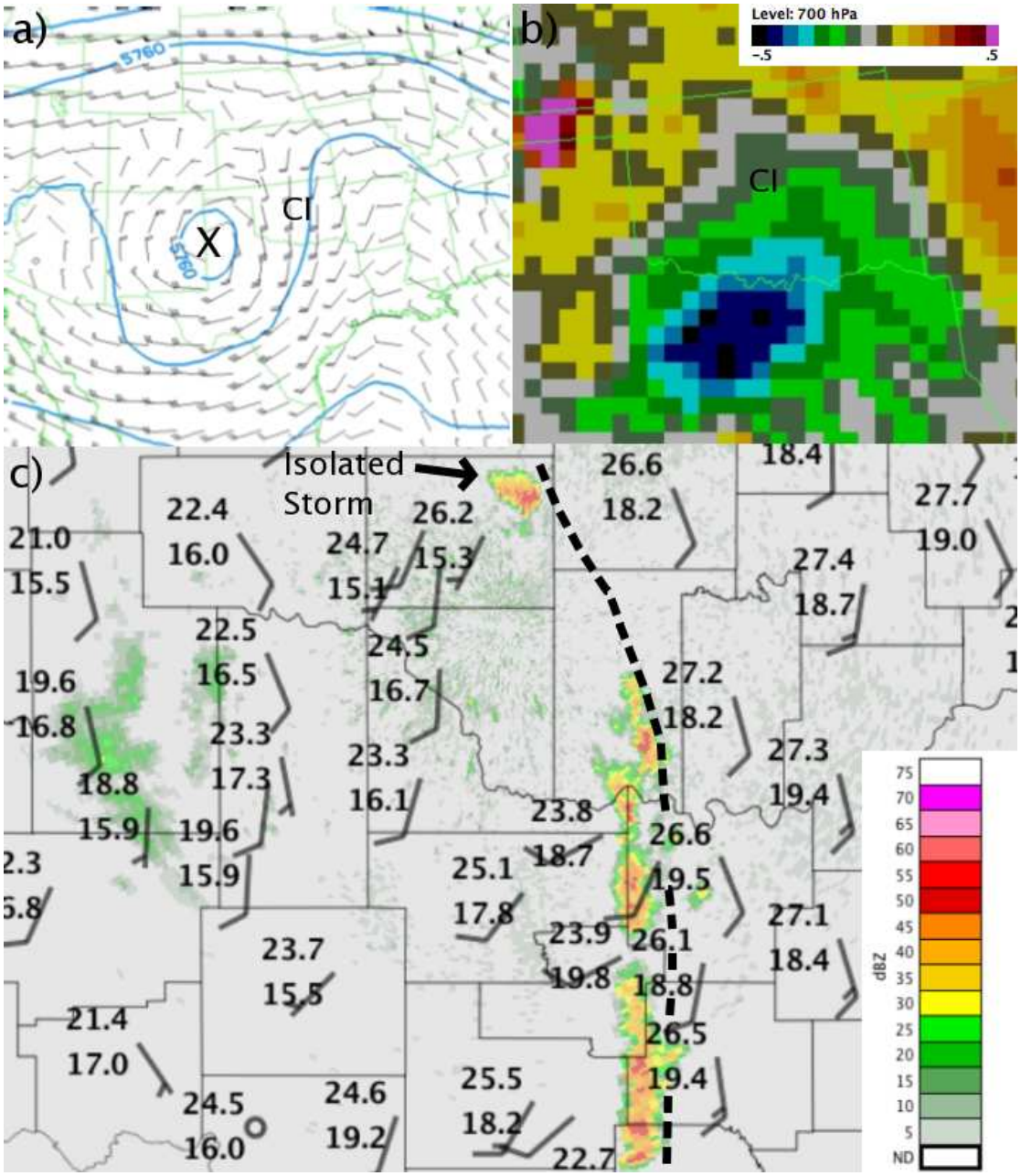

Figure 3: Plots from 30 April 2007 showing the a) RUC 500-hPa analysis at 1800 UTC, b) RUC 700-hPa vertical velocity field (Pa s^{-1}) at 1800 UTC, and c) surface and radar observations at 1825 UTC. The 500-hPa geopotential heights are contoured in solid blue lines at 60-m intervals, and wind barbs (m s^{-1}) showing wind speed and direction are plotted. The half barb and full barb represent a 2.5 m s^{-1} and 5 m s^{-1} wind speed, respectively. The black X denotes the vorticity maximum at 500 hPa. Mesonet temperature, dewpoint temperature, 10-m wind barb (m s^{-1}), and 0.5°-tilt reflectivity at 1825 UTC are plotted in the surface analysis. The black dashed line demarcates the mesoscale boundary, and the annotation CI shows the location of convection initiation.

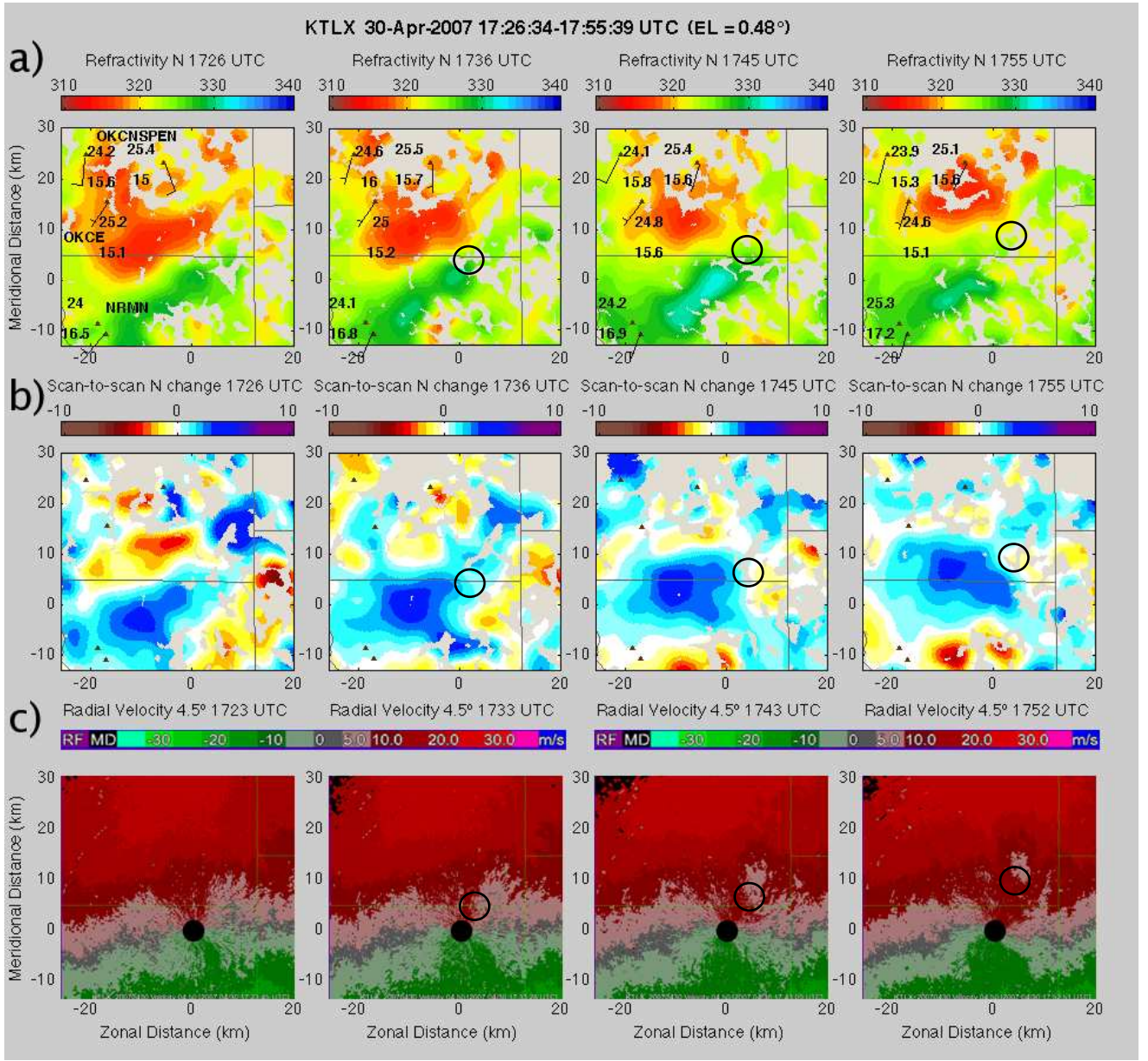

Figure 4: a) Refractivity, b) scan-to-scan refractivity change at 1726, 1736, 1745, and 1755 UTC 30 April 2007, and c) 4.5°-tilt radial velocity at 1723, 1733, 1743, and 1752 UTC 30 April 2007. The black circles on each field mark the location of the convergent signature in radial velocity associated with the updraft. Mesonet temperature, dewpoint temperature, and wind barb (same as Fig. 3) are plotted on the refractivity panels.

4.2. Convection Initiation

The three ingredients required for convection initiation are moisture, instability, and lift (McNulty, 1978; Doswell, 1987; Johns and Doswell, 1992). The relative humidity between the surface and 500 hPa was computed using sounding relative humidity data weighted by the depth of each measurement. The mean relative humidity value between the surface and 500 hPa was 55% for the 0000 UTC 30 April 2007 OUN sounding. The moderately high mean relative humidity between the surface and 500 hPa, and 15°C surface dewpoint temperatures provided sufficient moisture for convection initiation. Approximately 400–500 J kg^{-1} of convective available potential energy (CAPE, shown in forthcoming sounding analysis of a modified OUN sounding) provided sufficient instability for convection initiation, and mesoscale lift was provided by the MB. While it appears that all three ingredients for convection initiation were available, a high LFC and a small layer of CIN suggested that convection initiation was unlikely unless a source of lift to about 2000 m was present. This suggests that an enhancement in moisture or lift (or both) was necessary for convection initiation.

To confirm the hypothesis that the depth of lifting was insufficient to reach the LFC, the depth of lifting provided by the MB was estimated using the reflectivity difference, Z_{diff}, between the MB and the surroundings. Tracers (e.g., insects, dust) accumulate along convergent boundary updrafts (e.g., Wilson and Schreiber, 1986), increasing reflectivity within the convergent boundary updraft. Because microinsects tend to resist updraft motions (Geerts and Miao, 2005; Buban et al., 2007), higher reflectivity values may not necessarily be observed near the top of the boundary. Hence, this estimate of the depth of the MB is possibly an underestimate of the true depth of the MB.

To estimate the depth of the MB, the mean reflectivity along the fine line (Boundary Z) was computed and compared to the mean reflectivity of the two adjacent gates (Adjacent Z) on each side of the MB. The Z_{diff} threshold for determining if the MB extended through a particular level was set to 1 dB, which is the margin of error for reflectivity measurements for the WSR-88D (Chrisman and Chrisman, 1999). At 1811 UTC, 0.5°-tilt reflectivity values along the fine line ranged from 10 – 26 dBZ (Fig. 7a), and a vertical cross section of reflectivity (Fig. 7b) showed a maximum in reflectivity along the MB at the 0.5° and 1.5° tilts. Z_{diff} values of 8.8 and 7.2 dB were obtained at the 0.5° and 1.5° tilts, respectively, showing much higher reflectivity along the MB (Table 1). Smaller Z_{diff} values were still observed at the 2.5° and 3.4° tilts (Table 1), however the 3.4°-tilt Z_{diff} was below the Z_{diff} threshold. This suggests that the reflectivity difference became insignificant at the 3.4° tilt, so the maximum height of the MB based on this analysis is 1.3 km AGL.

Using the first 30-dBZ echo as the threshold for convection initiation (e.g., Wilson and Schreiber, 1986), convection initiation occurred at 1811 UTC at 2.5° elevation, though coherent reflectivity structures were observed as early as 1806 UTC at 1.5° elevation (not shown). The absence of enhanced reflectivity prior to 1806 UTC can be attributed to insufficient precipitation to produce an enhanced reflectivity structure. However, owing to mass continuity, storm-scale convergence is required to compensate for the developing updraft. Thus, storm-scale convergence can be assumed to be a precursor to the reflectivity-based definition of convection initiation.

A north-south cross section of the storm showed that storm-scale convergence extended through the lowest 2.5 km of the storm at 1811 UTC (Fig. 7d). Given the presence of clutter at lower tilts, radial velocity fields at 4.5° were examined further (1.1–1.4 km AGL). Storm-scale convergence was observed in the 4.5°-tilt radial velocity fields at 1733, 1743, and 1752 UTC (Fig. 4c), implying the presence of an updraft associated with the developing storm as early as 1733 UTC. The average computed convergence values (over 10–12 radially adjacent gates along convergence axis) ranged between 0.003 to 0.004 s^{-1} between 1733 and 1752 UTC. Although radial velocity data did not show storm-scale convergence prior to 1733 UTC, convergent flow was observed over a larger area between the NRMN Mesonet site and KTLX. At 1725 and 1735 UTC, southwesterly flow was observed at the NRMN Mesonet site, and south-southeasterly surface flow was evident from the 4.5° radial velocity field at 1723 and 1733 UTC (black dot in Fig. 4c).

The storm-scale convergence associated with the developing storm was located on the northeast side of the moisture pool at 1736 and 1745 UTC (Fig. 4), showing that the developing storm resided in a region with higher surface moisture. The moisture pool was located within the convergent flow observed prior to 1736 UTC, indicating increased moisture convergence prior to convection initiation. The moisture pool and convergent signature are closest at the earliest observation of storm-scale convergence, which is also presumably closest to the time when the initial updraft reaches the LFC (Fig. 4). The absence of storm-scale convergence suggests that a deep updraft was likely not present prior to 1733 UTC, which is a reasonable conclusion given that first echoes occurred about 30 minutes later. The increasing displacement of the moisture pool and developing storm with time is caused by differences in the velocity of the moisture pool and the developing storm.

To determine if the developing storm ingested the higher surface moisture, the near-surface storm-relative (SR) wind was computed using VAD data and storm motion computed from WDSSII. The average 1745 UTC VAD wind speed and direction at the lowest two levels (38 and 129 m) were 7.2

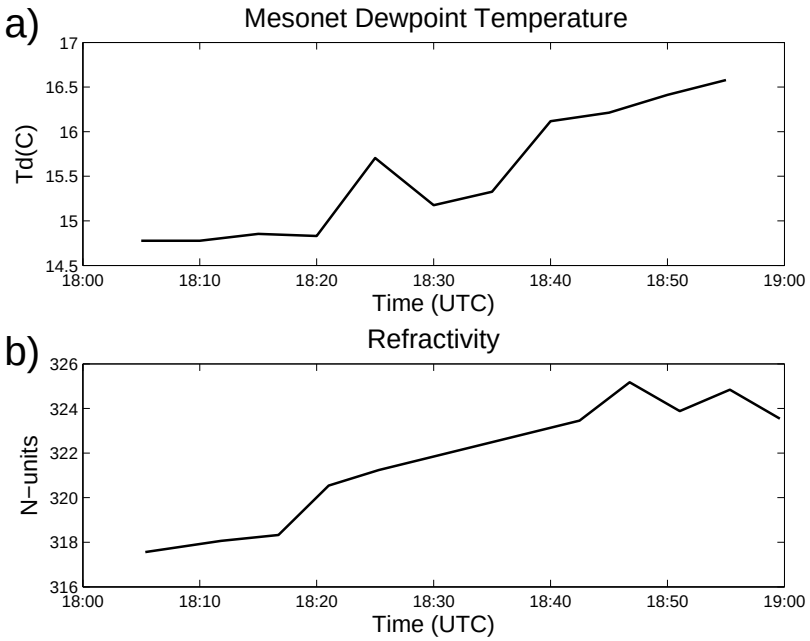

Figure 5: a) Time-series plot of SPEN dewpoint temperature, and b) radar refractivity measured at SPEN. The moisture pool passed between 1810 and 1845 UTC, as indicated by an increase in both dewpoint temperature and radar refractivity.

Table 1: Reflectivity difference, Z_{diff}, for multiple elevation angles providing a reflectivity comparison between the fine line (MB) and the adjacent gates. The elevation angle and the maximum heights above ground level are also provided.

Ele. Angle	Max. Height (km)	Boundary Z (dBZ)	Adjacent Z (dBZ)	Z_{diff} (dB)
0.5°	0.3	17.6	8.8	8.8
1.5°	0.6	9.2	2.0	7.2
2.5°	0.8	2.1	-0.4	2.5
3.4°	1.3	0.4	-0.5	0.9

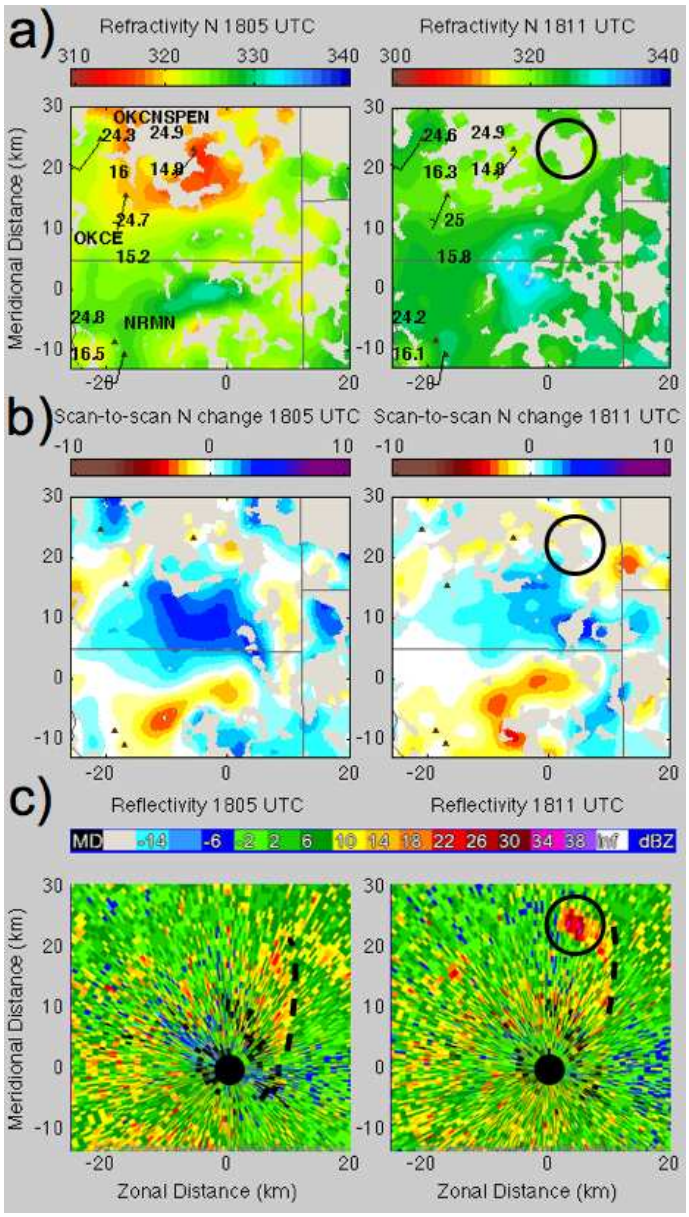

Figure 6: a) Refractivity, b) scan-to-scan refractivity change, and c) 0.5°-tilt reflectivity at 1805 and 1811 UTC 30 April 2007. In reflectivity, the isolated storm (black circle on each field) was evident just north of the moisture pool at 1811 UTC. The MB is demarcated by the black dashed line on the reflectivity field. Mesonet temperature, dewpoint temperature, and wind barb (same as Fig. 3) are plotted on the refractivity panels.

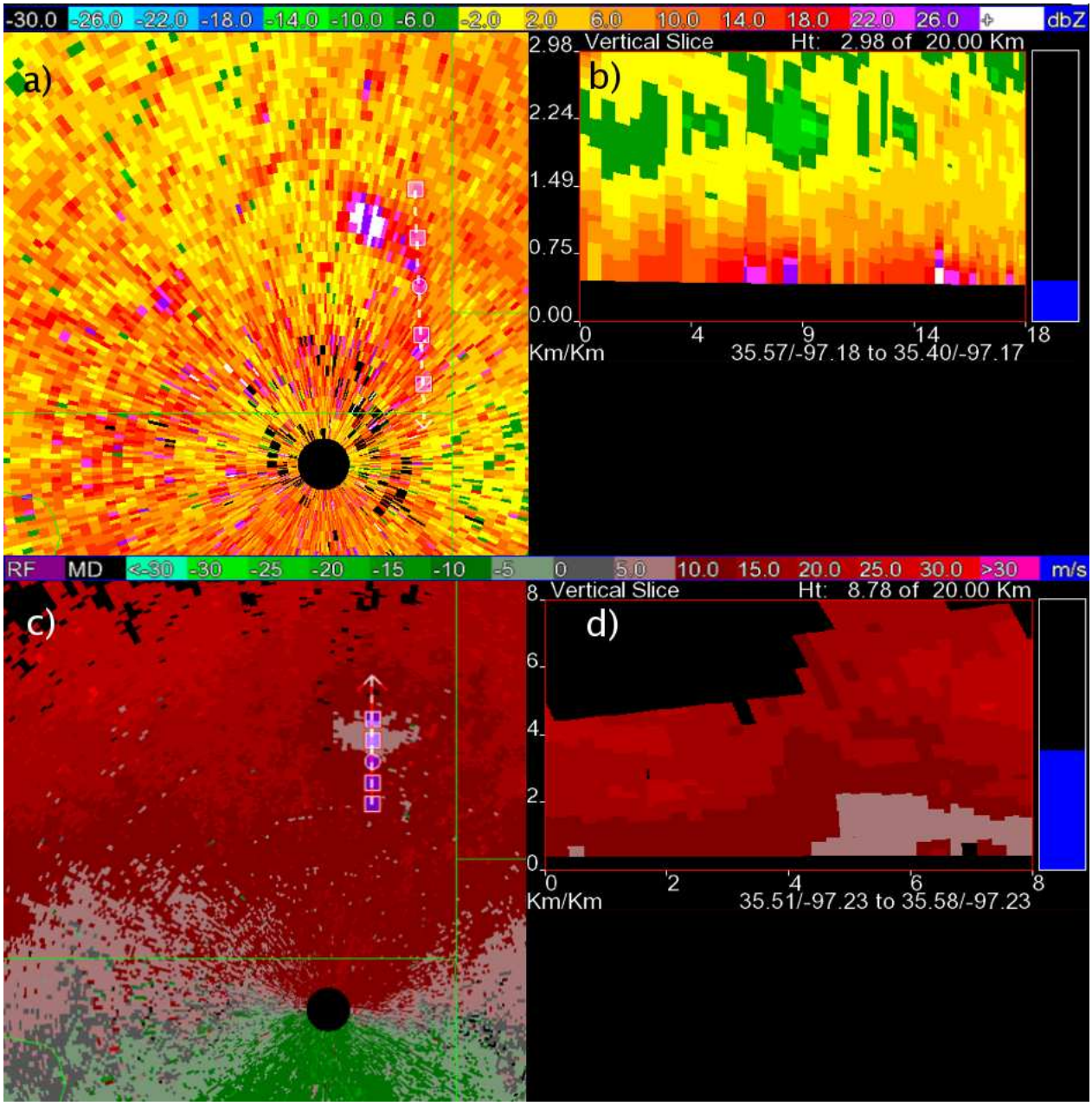

Figure 7: a) 0.5°-tilt reflectivity at 1811 UTC, b) cross section (18 km from north to south) of reflectivity along the fine line at 1811 UTC c) 2.4°-tilt radial velocity at 1812 UTC, d) cross section (8 km from south to north) of radial velocity at 1811 UTC. The reflectivity cross section along the MB shows reflectivity values between 10 and 25 dBZ along the fine line, and the cross section of radial velocity shows storm-scale convergence through about 2.5 km.

m s^{-1} and 201°, respectively. The magnitudes of near-surface SR wind were very small (Table 2), indicating that the storm was ingesting the higher moisture very close to the storm during the early stages of convection initiation. The next section investigates the impact of ingesting the higher moisture on convection initiation.

4.3. Impact of Moisture Variability on Convection Initiation

To assess the impact of moisture variability on convection initiation, NSHARP (Hart and Korotky, 1991) was used to modify soundings. Several upper-air observations were considered for the sounding analysis because upper-air observations were not available at the time and location of convection initiation. A 1800 UTC LMT sounding provided the most timely upper-air measurement, but was located 180 km from the convection initiation site. The closest soundings to the convection initiation location were the 1200 UTC 30 April 2007 and 0000 UTC 1 May 2007 OUN soundings. A 1700 UTC RUC sounding was also available near the site of convection initiation. However, the surface and boundary layer moisture values were too high compared to surface and upper-air observations, and the vertical resolution (50 hPa) was limited compared to the upper-air observations. From these data sources, the 1200 UTC 30 April 2007 and 0000 UTC 1 May 2007 OUN soundings were selected for further analysis given their spatial proximity to convection initiation.

The 1200 UTC 30 April 2007 and 0000 UTC 1 May 2007 OUN soundings exhibited similar temperature and dewpoint temperature profiles above the boundary layer. Nonetheless, the temperature and dewpoint temperature measurements from the 1200 UTC 30 April 2007 and 0000 UTC 1 May 2007 OUN soundings were averaged to better simulate the conditions at 1800 UTC 30 April 2007. The boundary layer temperature profile was then modified to well-mixed conditions through 900 hPa. This averaged sounding is shown in Fig. 8.

Three scenarios were created to investigate the impact of moisture variability on convection initiation. Scenario 1 was based on the average surface conditions from the Mesonet stations closest to the site of convection initiation (OKCE and SPEN) prior to convection initiation. Scenario 2 examined a 1.4°C dewpoint temperature increase based on the SPEN Mesonet dewpoint temperature change caused by the moisture pool. Scenario 3 investigated a 2°C increase in dewpoint temperature based on the observed radar refractivity change across the moisture pool. The averaged OUN sounding was further modified based on Scenarios 1–3 to create three new soundings, using the surface conditions listed in Table 3.

The modified sounding for Scenario 1 (Fig. 8) showed CIN of -22 J kg^{-1} (Table 3). The sounding analyses also revealed a high LFC of 2092 m (Fig. 9a). Given a limited depth of lift provided by the MB — up to 1300 m — and the higher LFC indicated by this analysis, convection initiation was unlikely without thermodynamic changes to lower the LFC and reduce CIN.

Scenarios 2 and 3 investigated the impact of moisture variability on the thermodynamic environment (Table 3). Based on the Mesonet-observed moisture increase associated with the moisture pool (Scenario 2), the moisture pool reduced CIN from -22 to -3 J kg^{-1} and the height of the LFC was reduced from 2092 to 1797 m (Fig. 9b). Based on the results for Scenario 2, the small residual CIN would likely not be sufficient to prevent a convergent updraft from penetrating through the stable layer, and the LFC would be lowered to within 497 m of the MB. Although the LFC remains above the depth of surface lifting, the absence of CIN may enable a convective updraft along the MB to reach the LFC. Considering the increase in moisture from the refractivity-based estimate (Scenario 3), the LFC was reduced from 2092 to 1015 m. The LFC was lowered to within the estimated maximum MB depth and CIN was expunged (Fig. 9c). Thus, the depth of lifting provided by the MB would be sufficient for convection initiation, and absence of CIN implies that a stable layer would no longer prevent a convective updraft from reaching the LFC. The 0000 UTC 1 May 2007 OUN sounding and the 1800 UTC 30 April 2007 LMT sounding were also modified based on these three scenarios, and similar results — lowering of LFC within MB depth and elimination of CIN — were obtained (not shown). This illustrates that the results in this section were independent of small differences among the soundings.

5. CONCLUSIONS

The 30 April 2007 case examined the effects of moisture variability on convection initiation in a synoptically active environment using radar refractivity retrievals to reanalyze soundings. Although the three ingredients for convection initiation were nearly sufficient, CIN and a high LFC above the depth of the MB suggested that convection initiation was unlikely. Thus, an enhancement in moisture or lift was necessary for convection initiation. Radar refractivity data showed relatively high, small-scale moisture variability associated with a moisture pool. Radial velocity data revealed that the developing storm was collocated with the moisture pool and the developing storm ingested the higher moisture. NSHARP was used to modify soundings to investigate the impact of moisture variability on convection initiation. The modified soundings showed that moisture variability enabled convection initiation within the moisture pool by reducing or eliminating CIN, and lowering the LFC to near or within the depth of lifting provided by the MB.

Table 2: Storm motion and SR flow computed using WDSSII and the average 1745 UTC VAD wind from the two lowest levels.

Times (UTC)	Storm Motion (m s^{-1}) /Direction (°)	SR Wind Speed (m s^{-1}) /Direction (°)
1733–1743 UTC	6.4/207	0.8/206
1743–1752 UTC	7.1/189	1.5/290

Table 3: Thermodynamic variables from modified sounding analyses for the OUN sounding.

Case	T (C)	T_d (C)	CIN (Jkg^{-1})	CAPE (Jkg^{-1})	LFC (m)	LCL (m)
Scenario 1	25	15	-22	492	2092	1265
Scenario 2	25	16.4	-3	997	1797	1091
Scenario 3	25	17	0	1230	1015	1015

This study corroborates modeling results from Crook (1996) and observational results from Weckwerth (2000), which found that impact of moisture variability is greatest at the convection initiation/no convection initiation boundary. This analysis showed that convection initiation was only supported thermodynamically within a local maximum in the moisture field. The study supports the work of Fabry (2006) by illustrating a case where the effects of moisture variability on convection initiation were greatest at scales less than 20 km. The moisture pool observed in refractivity and scan-to-scan refractivity possessed a wavelength of about 15–20 km, so moisture variability at scales less than 20 km was critical for this case. A case study using radar refractivity data to demonstrate the impact of a local maximum in the moisture field on a convection initiation event is also a unique aspect of this study. Previous refractivity case studies of convection initiation have focused on the relationship between increasing moisture gradients and convection initiation.

This case study revealed observational evidence that moisture variability in a synoptically active environment impacted convection initiation in the absence of boundaries with strong moisture gradients (e.g., dryline, outflow boundary). Previous observational studies have focused on the effects of moisture variability on convection initiation in quiescent conditions, or in the presence of boundaries with strong moisture gradients. While this study provides one example of the importance of moisture variability to convection initiation processes, the impact of moisture variability in different convective environments remains for further investigation. For example, what impact does moisture variability have on convection initiation for a convective environment with no CIN and a LFC within the depth of surface lifting?

While refractivity data exhibited utility for examining moisture variability and using measurements of moisture variability to assess if air can be lifted to the LFC, reaching the LFC is a necessary, but insufficient condition for convection initiation. The development of the storm after a convective updraft reaches the LFC depends on conditions that affect deep convection (e.g., instability, entrainment). Thus, the refractivity-observed moisture pool may have little impact after the air parcel is lifted to the LFC, especially after the storm moves away from the moisture pool. Hence, for convection initiation, the primary utility for refractivity data will be assessing if air can be lifted to the LFC, based on the observed moisture variability. Inferring the variability of CAPE based on moisture variability observed by refractivity data could potentially improve estimates of updraft strength and the likelihood of deep convection. In this study, the storm resided in a region of higher moisture which may explain why an intense storm developed, even though CAPE values where convection initiation ensued were relatively low. Although the developing storm eventually moved into a drier environment, CAPE remained sufficient for continuance of convection initiation.

The case study illustrated the capability of radar refractivity data to resolve sub-observational-scale moisture variability. Refractivity data showed that significant moisture variability can occur between Mesonet stations, suggesting that refractivity data could be a useful surrogate data source for small-scale moisture variability. Although the Mesonet data showed an increase in moisture associated with the moisture pool, the spatial extent of the moisture pool is poorly resolved whereas radar refractivity data clearly demarcated the spatial structure of the moisture pool. The refractivity data revealed that the moisture pool and initial storm updraft were collocated, whereas these observations could only be speculated using the nearest surface station. Although there is a growing impetus for higher resolution surface mesonets, few states have a good surrogate surface network to the ASOS network. The results from this study and previous studies (e.g., Heinselman et al., 2009) suggest that

refractivity data would have even greater utility in locations without mesonets, because the typical refractivity domain (about 80-km wide) will only have one ASOS station, based on the 90-km average spacing of ASOS stations.

6. ACKNOWLEDGMENTS

Funding for this research was provided by the Radar Operations Center through grant number NA17RJ1227 and the National Science Foundation through grant number ATM0750790. The first author was supported by an American Meteorological Society Fellowship sponsored by the Raytheon Corporation. This paper benefited from reviews by Conrad Ziegler and Rodger Brown, and discussions with Conrad Ziegler. The authors thank the Radar Operations Center for maintaining the data flow from KTLX during the experiment. The authors would thank Mark Laufersweiler, Kevin Manross, and Travis Smith for their assistance with data acquisition and computing support.

References

Bean, B. R., and E. J. Dutton, 1968: *Radio Meteorology*. Dover Publications, 435 pp.

Benjamin, S. G., D. Devenyi, S. S. Wegandt, K. J. Brundage, J. M. Brown, G. A. Grell, D. Kim, B. E. Schwartz, T. G. Smirnova, T. L. Smith, and G. S. Manikin, 2004: An hourly assimilation/forecast cycle: The RUC. *Mon. Wea. Rev.*, **132**, 495–518.

Bodine, D., P. L. Heinselman, B. L. Cheong, R. D. Palmer, and D. Michaud, 2008: Convection initiation and storm evolution forecasting using radar refractivity retrievals. in *24th Conf. on Severe Local Storms*.

Bodine, D., P. L. Heinselman, B. L. Cheong, R. D. Palmer, and D. Michaud, 2009a: Radar refractivity applications for convective initiation forecasting and observations of the convective boundary layer. in *25th Conference on IIPS*, Phoenix, AZ.

Bodine, D., R. D. Palmer, B. L. Cheong, P. L. Heinselman, D. S. Michaud, and G. Zhang, 2009b: Can high-resolution surface moisture fields be retrieved in supercells? in *34th Conf. on Radar Meteorology*, Williamsburg, VA.

Brock, F. V., K. C. Crawford, R. L. Elliott, G. W. Cuperus, S. J. Stadler, H. L. Johnson, and M. D. Eilts, 1995: The Oklahoma Mesonet: A technical overview. *J. Atmos. Oceanic Technol.*, **12**, 5–19.

Buban, M., C. Ziegler, E. Rasmussen, and Y. Richardson, 2007: The dryline on 22 May 2002 during IHOP: Ground-radar and in situ data analyses of the dryline and boundary layer evolution. *Mon. Wea. Rev.*, **135**, 2473–2505.

Cheong, B. L., R. D. Palmer, C. D. Curtis, T.-Y. Yu, D. S. Zrnić, and D. Forsyth, 2008: Refractivity retrieval using the Phased Array Radar: First results and potential for multi-function operation. *IEEE Tran. Geosci. Remote Sensi.*, **46**, 2527–2537.

Chrisman, J., and C. Chrisman, 1999: An operational guide to WSR-88D reflectivity data quality assurance. WSR-88D Radar Operations Center paper, Radar Operations Center, 120 David L. Boren Blvd., Norman, OK 73072.

Crook, A. N., 1996: Sensitivity of moist convection forced by boundary layer processes to low-level thermodynamic fields. *Mon. Wea. Rev.*, **124**, 1767–1785.

Dabberdt, W. F., and T. W. Schlatter, 1996: Research opportunities from emerging atmospheric observing and modeling capabilities. *Bull. Amer. Meteor. Sci.*, **77**, 305–323.

Demoz, B., C. Flamant, T. Weckwerth, D. Whiteman, K. Evans, F. Fabry, P. Girolamo, D. Miller, B. Geerts, W. Brown, G. Schwemmer, B. Gentry, W. Feltz, and Z. Wang, 2006: The dryline on 22 May 2002 during IHOP: Convective-scale measurements at the profiling site. *Mon. Wea. Rev.*, **134**, 294–310.

Doswell, C. A., 1987: The distinction between large-scale and mesoscale contribution to severe convection: A case study example. *Wea. Forecasting*, **2**, 3–16.

Emanuel, K., K. D. Raymond, A. Betts, L. Bosart, C. Bretherton, K. Droegemeier, B. Farrell, J. M. Fritsch, R. Houze, M. LeMone, D. Lilly, R. Rotunno, M. Shapiro, R. Smith, and A. Thorpe, 1995: Report of first prospectus development team of the U.S. Weather Research Program to NOAA and the NSF. *Bull. Amer. Meteor. Sci.*, **76**, 1194–1208.

Fabry, F., 2004: Meteorological value of ground target measurements by radar. *J. Atmos. Oceanic Technol.*, **21**(4), 560–573.

Fabry, F., 2006: The spatial variability of moisture in the boundary layer and its effect on convective initiation: Project-long characterization. *Mon. Wea. Rev.*, **134**, 79–91.

Fabry, F., C. Frush, I. Zawadzki, and A. Kilambi, 1997: On the extraction of near-surface index of refraction using radar phase measurements from ground targets. *J. Atmos. Oceanic Technol.*, **14**(4), 978–987.

Geerts, B., and Q. Miao, 2005: A simple numerical model of the flight behavior of small insects in the atmospheric convective boundary layer. *Environ. Entomol.*, **34**, 353–360.

Hart, J. A., and W. Korotky, 1991: The sharp workstation vl.50 users guide. Tech. rep., NOAA/National Weather Service, Eastern Region Headquarters, 630 Johnson Ave., Bohemia, NY 11716.

Heinselman, P. L., B. L. Cheong, R. D. Palmer, D. Bodine, and K. Hondl, 2009: Radar refractivity retrievals from KTLX: Insights into operational benefits and limitations. *Wea. Forecasting*, in press.

Johns, R. H., and C. A. Doswell, 1992: Severe local storms forecasting. *Wea. Forecasting*, **7**, 588–612.

Koch, S. E., and S. Saleeby, 2001: An automated system for the analysis of gravity waves and other mesoscale phenomena. *Wea. Forecasting*, **16**, 661–679.

Lakshmanan, V., T. Smith, G. J. Stumpf, and K. Hondl, 2007: The Warning Decision Support System - Integrated Information. *Wea. Forecasting*, **22**, 596–612.

Lee, B. D., R. D. Farley, and M. R. Hjelmfelt, 1991: A numerical case study of convection initiation along colliding convergence boundaries in Northeast Colorado. *J. Atmos. Sci.*, **48**, 2350–2366.

McLaughlin, D., D. Pepyne, V. Chandrasekar, B. Philips, J. Kurose, M. Zink, K. Droegemeier, S. Cruz-Pol, F. Junyent, J. Brotzge, D. Westbrook, N. Bharadwaj, Y. Wang, E. Lyons, K. Hondl, Y. Liu, E. Knapp, M. Xue, A. Hopf, K. Kloesel, A. DeFonzo, P. Kollias, K. Brewster, R. Contreras, T. Djaferis, E. Insanic, S. Frasier, and F. Carr, 2009: Short-wavelength technology and the potential for distributed networks of small radar systems. *Bull. Amer. Meteor. Sci.*, in press.

McNulty, R. P., 1978: On upper tropospheric kinematics and severe weather occurence. *Mon. Wea. Rev.*, **106**, 662–672.

McPherson, R. A., C. A. Fiebrich, K. C. Crawford, J. R. Kilby, D. L. Grimsley, J. E. Martinez, J. B. Basara, B. G. Illston, D. A. Morris, K. A. Kloesel, A. D. Melvin, H. Shrivastava, J. M. Wolfinbarger, J. P. Bostic, and D. B. Demko, 2007: Statewide monitoring of the mesoscale environment: A technical update on the Oklahoma Mesonet. *J. Atmos. Oceanic Technol.*, **24**, 301–321.

National Research Council, 1998: *The Atmospheric Sciences: Entering the Twenty-First Century*. National Academy Press, pp. 373.

Parsons, D. B., M. A. Shapiro, and E. Miller, 2000: The mesoscale structure of a nocturnal dryline and of a frontal-dryline merger. *Mon. Wea. Rev.*, **128**, 3824–3838.

Roberts, R. D., F. Fabry, P. C. Kennedy, E. Nelson, J. Wilson, N. Rehak, J. Fritz, V. Chandrasekar, J. Braun, J. Sun, S. Ellis, S. Reising, T. Crum, L. Mooney, R. Palmer, T. Weckwerth, and S. Padmanabhan, 2008: REFRACTT-2006: Real-time retrieval of high-resolution low-level moisture fields from operational NEXRAD and research radars. *Bull. Amer. Meteor. Sci.*, **89**, 1535–1548.

Wakimoto, R. M., and H. V. Murphey, 2008: Analysis of a dryline during IHOP: Implications for convection initiation. *Mon. Wea. Rev.*, **137**, 912–936.

Weckwerth, T. M., 2000: The effect of small-scale moisture variability on thunderstorm initiation. *Mon. Wea. Rev.*, **128**, 4017–4029.

Weckwerth, T. M., D. B. Parsons, S. E. Koch, J. A. Moore, M. A. LeMone, B. B. Demoz, C. Flamant, B. Geerts, J. Wang, and W. F. Feltz, 2004: An overview of the International H20 Project (IHOP) and some preliminary highlights. *Bull. Amer. Meteor. Sci.*, **85**, 253–277.

Weckwerth, T. M., C. R. Pettet, F. Fabry, S. Park, M. A. LeMone, and J. W. Wilson, 2005: Radar refractivity retrieval: Validation and application to short-term forecasting. *J. Appl. Meteorol.*, **44**(3), 285–300.

Weckwerth, T. M., J. W. Wilson, and R. M. Wakimoto, 1996: Thermodynamic variability within the convective boundary layer due to horizontal convective rolls. *Mon. Wea. Rev.*, **124**, 769–784.

Wilson, J. W., and W. E. Schreiber, 1986: Initiation of convective storms at radar-observed boundary-layer convergence lines. *Mon. Wea. Rev.*, **114**, 2516–2536.

Ziegler, C. L., T. J. Lee, and R. A. Pielke, 1997: Convective initiation at the dryline: A modeling study. *Mon. Wea. Rev.*, **125**, 1001–1026.

Ziegler, C. L., and E. N. Rasmussen, 1998: The initiation of moist convection at the dryline: Forecasting issues from a case study perspective. *Wea. Forecasting*, **13**, 1106–1131.

Zrnić, D. S., J. F. Kimpel, D. E. Forsyth, A. Shapiro, G. Crain, R. Ferek, J. Heimmer, W. Benner, T. J. McNellis, and R. J. Vogt, 2007: Agile-beam phased array radar for weather observations. *Bull. Amer. Meteor. Sci.*, **88**, 1753–1766.

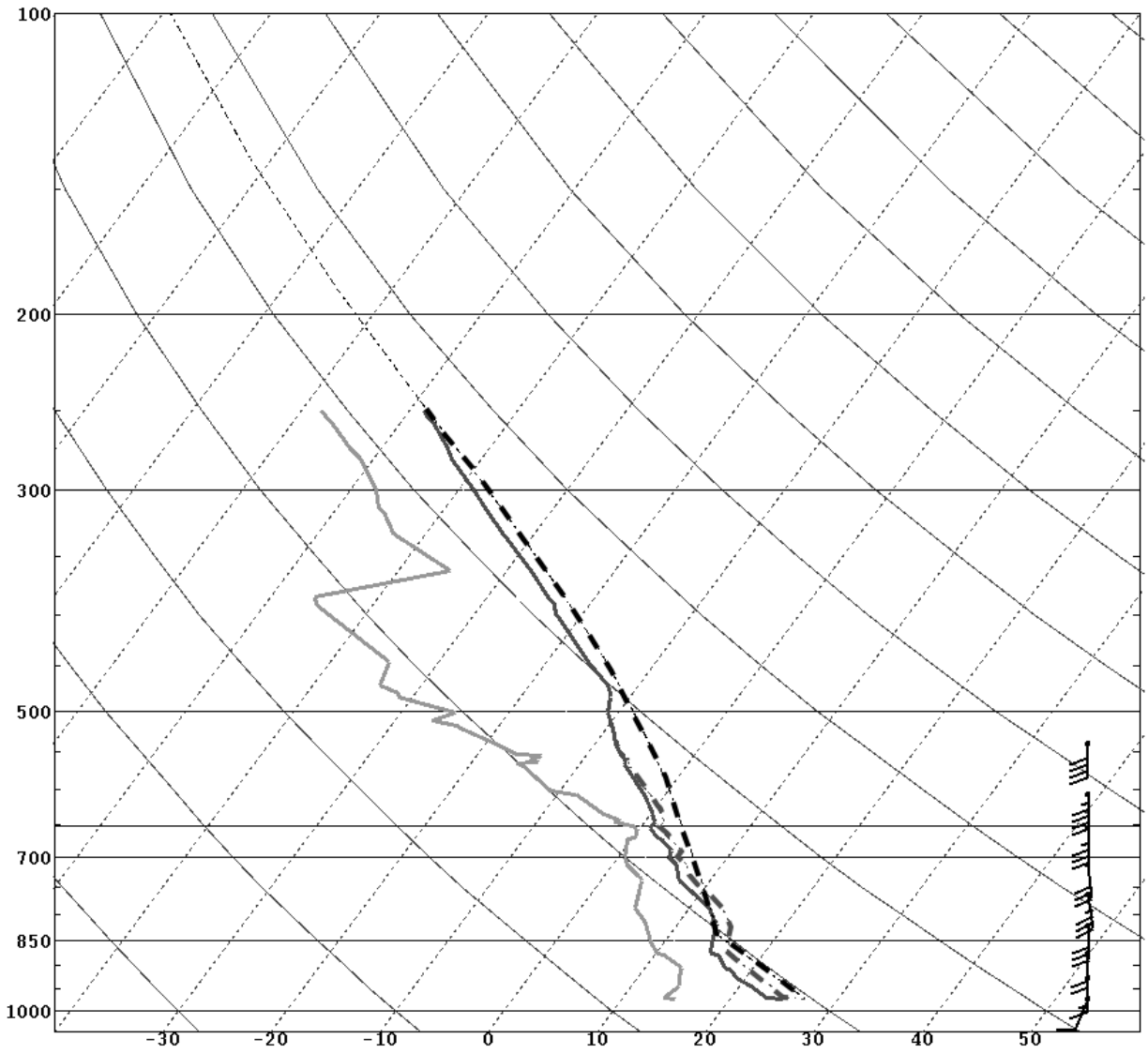

Figure 8: The averaged OUN sounding for Scenario 1 (T=25°C and T_d=15°C). The dewpoint temperature (solid light gray line), and temperature (solid dark gray line) profiles are plotted on the sounding. The dashed dark gray line indicates the modified environmental temperature, and the dashed black line indicates the parcel temperature. The 1745 VAD wind profile is plotted using wind barbs at the corresponding height (same as Fig. 3).

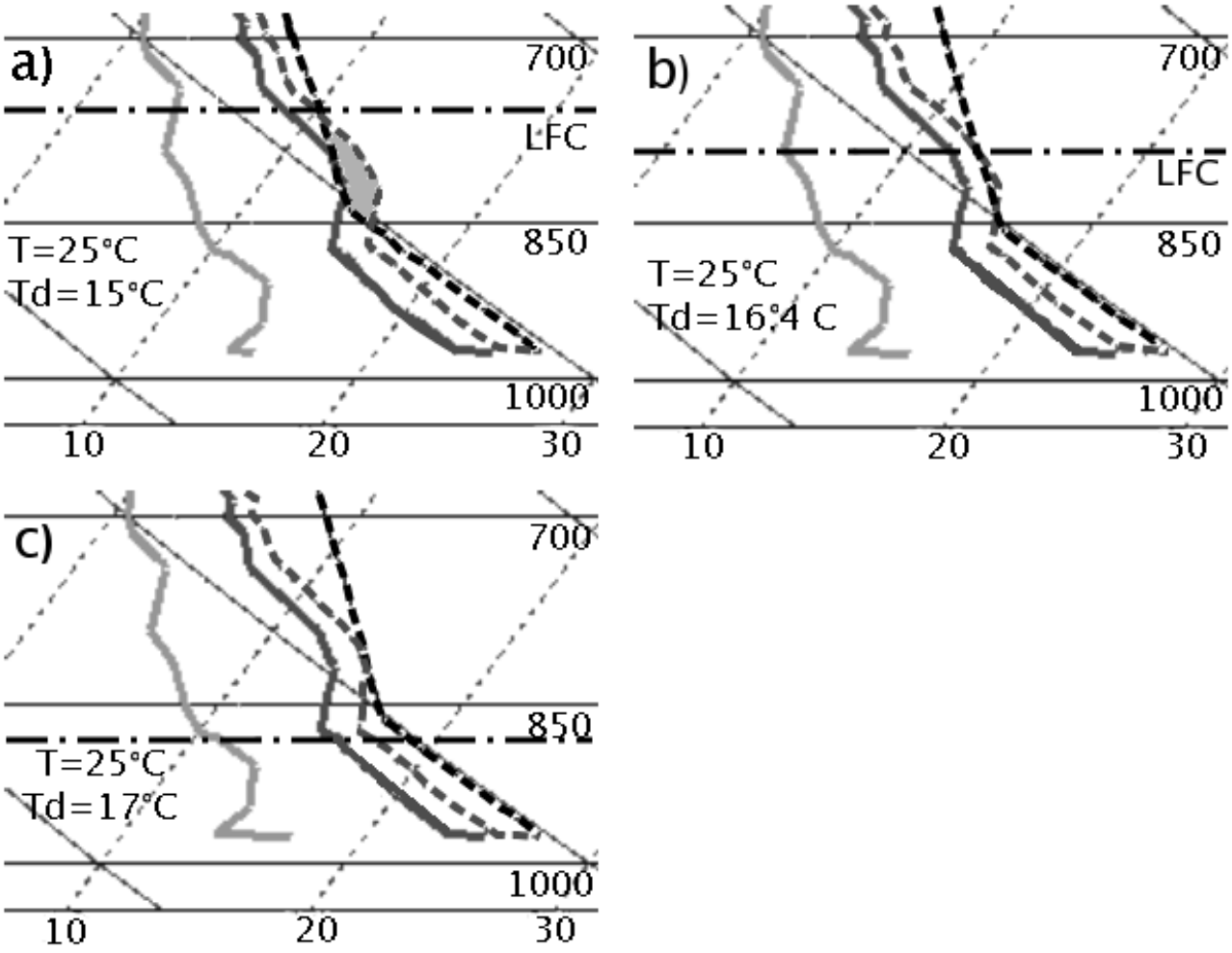

Figure 9: The averaged OUN sounding, further modified to simulate the impact of moisture variability near the convection initiation site. Soundings a) through c) correspond to Scenarios 1 through 3, where a) T=25°C and T_d=15°C, b) T=25°C and T_d=16.4°C, and c) T=25°C and T_d=17°C. The temperature, dewpoint temperature, modified environmental temperature, and parcel temperature are the same as Fig. 8. The shaded area delineates the area of CIN, and the LFC is annotated with a dashed-dotted black line.